Volume 16 | Number 4 | April 2014 | Pages 615–944

# Environmental Science Processes & Impacts

rsc.li/process-impacts

ISSN 2050-7887

ROYAL SOCIETY OF CHEMISTRY

PAPER
Beat Müller *et al.*
Early diagenetic processes generate iron and manganese oxide layers in the sediments of Lake Baikal, Siberia

Environmental Science Processes & Impacts

PAPER



Cite this: *Environ. Sci.: Processes Impacts*, 2014, **16**, 879

# Early diagenetic processes generate iron and manganese oxide layers in the sediments of Lake Baikal, Siberia

Natascha T. Torres,[ab] Lawrence M. Och,[a] Peter C. Hauser,[b] Gerhard Furrer,[c] Helmut Brandl,[d] Elena Vologina,[e] Michael Sturm,[f] Helmut Bürgmann[a] and Beat Müller*[a]



Received 10th December 2013
Accepted 30th January 2014

DOI: 10.1039/c3em00676j

rsc.li/process-impacts

Distinct layers of iron(III) and manganese(IV) (Fe/Mn) oxides are found buried within the reducing part of the sediments in Lake Baikal and cause considerable complexity and steep vertical gradients with respect to the redox sequence. For the on-site investigation of the responsible biogeochemical processes, we applied filter tube samplers for the extraction of sediment porewater combined with a portable capillary electrophoresis instrument for the analyses of inorganic cations and anions. On the basis of the new results, the sequence of diagenetic processes leading to the formation, transformation, and dissolution of the Fe/Mn layers was investigated. With two exemplary cores we demonstrate that the dissolution of particulate Fe and Mn is coupled to the anaerobic oxidation of $CH_4$ (AOM) either *via* the reduction of sulphate ($SO_4^{2-}$) and the subsequent generation of Fe(II) by S(−II) oxidation, or directly coupled to Fe reduction. Dissolved Fe(II) diffuses upwards to reduce particulate Mn(IV) thus forming a sharp mineral boundary. An alternative dissolution pathway is indicated by the occurrence of anaerobic nitrification of $NH_4^+$ observed at locations with Mn(IV). Furthermore, the reasons and consequences of the non-steady-state sediment pattern and the resulting redox discontinuities are discussed and a suggestion for the burial of active Fe/Mn layers is presented.

### Environmental impact

Early diagenetic processes in sediments lead to the formation of distinct accumulations of particulate Fe and Mn at the oxic–anoxic interface. Using on-site porewater measurements of Mn(II), Fe(II), $NH_4^+$, $NO_3^-$, and $SO_4^{2-}$ and later analysis of the solid phase for Mn and Fe, we hypothesize that these layers accumulated with the growing sediment but at some point were halted and subsequently buried in the sediment. This unique pattern of incidental burials of oxidized layers in the reducing (methanogenic) sediment introduces considerable heterogeneities and leads to very unusual diagenetic redox reactions. This manuscript provides the first concise description of the entire diagenetic sequence of processes induced by the Fe/Mn layers from (i) the formation of the Fe/Mn accumulations at the oxic–anoxic interface, (ii) the reductive dissolution of buried layers, and (iii) mechanisms leading to the burial of Fe/Mn layers.

## 1 Introduction

Lake Baikal is probably the oldest (30–40 Ma[1]), and, with a maximum depth of 1637 m, the deepest and the most voluminous lake in the world. The lake is situated on an active continental rift in southeastern Siberia, the Baikal Rift Zone, separating the Siberian craton in the northwest from the Mongolian–Transbaikalian belt in the southeast *e.g.* ref. 1. The proceeding deepening and the high age of the lake are ultimately the reasons for sedimentary deposits of over 7 km depth, which provide an invaluable archive of geological information often used to reconstruct long-term environmental changes, such as paleoclimate.[2–4] The oligotrophic character of the lake[5] and its pervasively oxygenated water column lead to unusually deep $O_2$ penetration into the sediment of up to 20 cm.[6]

A special feature of Lake Baikal sediments is the up to 3 cm thick layers of Fe and Mn oxides buried within the reducing part of the sediments and deposited on the deeper plains of all three sub-basins of the lake.[3,7] The origin and the dynamics of the Fe/Mn layers have been hypothesized to be caused by past climate changes[3,8] or tectonic rift events and the ensuing redistribution of Fe and Mn.[9] The Fe/Mn layers cause considerable vertical

[a]Eawag, Swiss Federal Institute of Aquatic Science and Technology, CH-6047 Kastanienbaum, Switzerland. E-mail: beat.mueller@eawag.ch
[b]Department of Chemistry, University of Basel, CH-4056 Basel, Switzerland
[c]Institute of Biogeochemistry and Pollution Dynamics, ETH Zurich, CH-8092 Zürich, Switzerland
[d]Institute of Evolutionary Biology and Environmental Studies, University of Zürich, CH-8057 Zurich, Switzerland
[e]Institute of Earth's Crust, Siberian Branch of RAS, Irkutsk, 664033, Russia
[f]Eawag, Swiss Federal Institute of Aquatic Science and Technology, CH-8600 Dübendorf, Switzerland

discontinuities in the redox sequence commonly observed in sediments[10] and are associated with the diagenetic redistribution of elements such as P, Ca, Sr, As, Sb, and some trace metals.[11] While suggestions for the processes of formation and transformation of Fe/Mn layers at the oxic–anoxic interface were brought forward by Müller *et al.*[11] and Och *et al.*,[12] the ultimate cause for occasional burial is still not clarified. Although some mechanisms have been proposed, such as changes in either the mass accumulation rate of organic carbon, sedimentation rate, porosity, or $O_2$ supply to the sediment, no conclusive evidence has yet been found.

Och *et al.*[12] hypothesized a cycle characterized by the dynamic growth of Fe and Mn oxide layers right underneath the depth of maximum $O_2$ penetration, an increasingly slowed down reductive dissolution followed by the burial of the Fe/Mn oxide accumulation and the subsequent initiation of a new dynamic Fe/Mn layer above. Ultimately, the dissolution of the buried Fe/Mn oxide layer is controlled by the anaerobic oxidation of $CH_4$ (AOM) by $SO_4^{2-}$ and/or Fe oxides in the deeper sediment, and the formation of the upper dynamic Fe/Mn oxide layer by the diffusive flux of $O_2$ from the water column into the sediment.

Until now, investigating the complex redox chemistry of the Lake Baikal sediments has been limited by the laborious porewater sampling, sampling artefacts such as contamination or the oxidation of dissolved Fe(II), small sample volumes and low concentrations restricting the number of analyses, as well as conservation and transport of the samples. Recently developed portable equipment,[13–15] consisting of MicroRhizon tubes and a portable capillary electrophoresis (CE) instrument,[13,16] allowed determination of *in situ* porewater data with high spatial resolution. Based on these high-quality data, we

• present the processes leading to the formation and transformation of the Fe/Mn layers on the basis of sediments and porewater analyses,

• discuss the reasons and consequences of the non-steady-state situation in the diagenetic process and the discontinuous redox sequence within the Lake Baikal sediments, and

• suggest possible causes for the burial of dynamically accumulating surface Fe/Mn layers into deeper sediments.

# 2 Materials and methods

## 2.1 Sampling site and sediment coring

Sediment cores were collected in March 2013 from two sites in the south basin of Lake Baikal (geographic positions: N 51°46′04.2″, E 104°24′33.8″ and N 51°41′33.8″, E 104°18′00.1″) (Fig. 1). The locations were accessed on the ice by a truck equipped with a winch for coring. Ice holes with a diameter of approximately 20 cm were drilled with an engine-driven wimble through the 90 cm thick ice layer to get access to the sediments at 1360 m depth, 14.4 km from the shore (core Baik13-4D, internal codes 'site A' or 'core A') and 3.8 km from the shore (core Baik13-6B, internal codes 'site B' or 'core B'). The following investigations were carried out:

1[st] core: porewater analysis & solid phase concentration measurements (site A, site B).

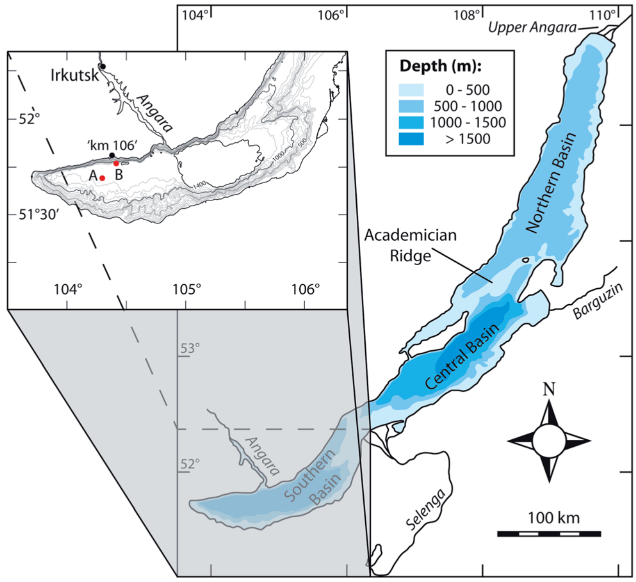


Fig. 1 Map of Lake Baikal and a zoom into the Southern Basin relief. The coring sites A and B are indicated by red dots. Base camp (Neutrino station) was at the shore of the lake near the station 'km 106' of the Circum-Baikal Railway.

2[nd] core: methane analyses (site A, site B).

3[rd] core: lithology & magnetic susceptibility, photograph (site A, site B).

4[th] core: XRF & microbial analyses (site A).

Cores were collected using a UWITEC gravity corer (UWITEC, Mondsee, Austria) with PVC tubes of 6.3 cm diameter and 60 cm length. Tubes for porewater sampling had holes of 0.15 cm diameter drilled staggered with a vertical resolution of 0.25 cm, while tubes for methane samples had holes of 1 cm diameter staggered with a vertical resolution of 1 cm. Modified liners were sealed with tape before coring that was cut open for sampling after retrieval. After the porewater sampling, both cores A and B were extruded in slices of 0.5 cm thickness for the uppermost 15 cm of the sediment and 1 cm thickness for the remaining lower part and transported to Switzerland for sediment analyses. One undisturbed core (only from site A) was transported to Switzerland for the microbial and XRF analyses, and one undisturbed core of each site was transported to the Russian Institute of Earth's Crust for detailed lithological analyses and measurement of the magnetic susceptibility.

Samples for $CH_4$ analyses were collected immediately after core retrieval. To prevent freezing (air temperature −20 °C) all the other collected sediment cores were immediately brought to the base camp to the improvised laboratories, which were heated to ~15 °C. Electricity was available from the close-by Circum-Baikal Railway line (kilometer 106).

## 2.2 Porewater sampling and analyses

Equipment for on-site porewater analyses, methane sampling, and sediment extrusion was packed in two boxes and carried on the plane as cabin luggage. We used two portable CE instruments for simultaneous on-site determination of cations and anions.[13,15] All solutions used for the sediment porewater analyses were prepared and ultrasonicated for 30 minutes at Eawag (Switzerland). Chemicals were of p.a. grade (Sigma-Aldrich, Steinheim, Germany or Fluka, Buchs, Switzerland) and only used with high purity deionized water (Purelab Ultra, ELGA LabWater, UK). The stock solutions of cations were prepared from the corresponding chloride salts. The stock solutions of anions were prepared from the corresponding sodium or potassium salts. Iron(II) standard solutions were prepared in $10^{-4}$ M HCl (Suprapur©, Merck, Darmstadt, Germany).

The whole equipment for the extraction and analyses of the porewater was set-up at the Neutrino station on the shore of Lake Baikal in the improvised laboratories on two simple working desks and connected to the local power supply. Porewater samples were retrieved from the cores immediately after arrival from the sampling site with MicroRhizon filter tube samplers of 2 cm length, 1–1.1 mm diameter and 0.15–0.20 μm pore size (Rhizosphere Research Products, Wageningen, Netherlands). They were connected to a 1 ml syringe and inserted horizontally into the staggered holes of the corer to draw 10 to 30 μl of porewater from the sediment. The samples were transferred to 1 ml PE centrifuge tubes and immediately injected into the portable CE instrument for measurement. Blanks (high purity deionized water collected with MicroRhizon samplers) and certified multi-element ion chromatography standard solutions (Fluka, Buchs, Switzerland) were intermittently measured to ensure a high data quality. The relative standard deviations of triplicate sample measurements were <5% for each ion.

For the data acquisition TraceDec® $C^4D$ detectors (Innovative Sensor Technologies GmbH, Strasshof, Austria) were used and the signals were recorded with the TraceMon software application. The peaks were analyzed using the Chart Software (version 5.5.8) from eDAQ (Denistone East NSW 2112, Australia). Fused silica capillaries (50 μm i.d., 360 μm o.d., 55 cm length) (BGB Analytik AG, Böckten, Switzerland) were used for separation. The capillaries were preconditioned with 1 M NaOH for 5 minutes, rinsed with high purity deionized water for 5 minutes, preconditioned with 1 M HCl for 5 minutes, rinsed again with high purity deionized water for 5 minutes, and finally equilibrated with the electrolyte solution for at least 30 minutes. A voltage of 15 kV was applied to the buffer vials. The sample was injected hydrodynamically by elevating the capillary end immersed in the sample vial for an injection time of 20 seconds at 15 cm height for anions and 8 cm for cations. The sampling and measurement of one sampling point was accomplished in maximum 15 minutes. Eight cations ($NH_4^+$, $K^+$, $Ca^{2+}$, $Na^+$, $Mg^{2+}$, $Mn^{2+}$, $Fe^{2+}$, and $Li^+$) and six anions ($Cl^-$, $NO_3^-$, $SO_4^{2-}$, $NO_2^-$, $F^-$, and $PO_4^{3-}$) were fully detected in less than ten minutes from an undiluted and immediately injected sample. Data evaluation and preliminary interpretation were done on the same day and therefore a maximum of flexibility in decision-making for further coring was provided on-site.

### 2.3 Additional analyses and procedures

**Methane.** Samples for $CH_4$ measurements were taken immediately after coring on the ice. Sediment sub-cores of 2 $cm^3$ volume were collected by insertion of a plastic syringe that was cut open at the tip through the pre-drilled holes. The tape covering the holes was cut open with a knife. The sub-samples were subsequently transferred into a serum flask containing 2 ml of 10 M NaOH and sealed with a butyl septum stopper. $CH_4$ was determined by headspace analyses with an Agilent gas chromatograph (Agilent Technologies AG, Basel, Switzerland) equipped with a Supelco Carboxene®-1010 column (Sigma-Aldrich, Steinheim, Germany), at the Eawag laboratory in Switzerland.

**Water content and porosity.** The water content was determined by weight difference before and after freeze-drying. The porosity ($\phi$) was estimated using an empirical relationship comprising TOC and water content.[5]

**Solid phase analyses.** The extruded sediment samples were freeze-dried and ground in an agate mortar at Eawag. Fe and Mn were determined after oxidative digestion (4 ml $HNO_3$ conc. and 1 ml $H_2O_2$ in a microwave oven for 30 minutes) with an ICP-MS (Agilent 7500 series, Agilent Technologies AG, Basel, Switzerland). Total carbon (TC) and total sulphur (TS) were determined by thermic combustion using an element analyzer, Euro EA 3000 (HEKAtech, Wegberg, Germany). Total inorganic carbon (TIC) was determined using a coulometer (CM5015, UIC, Joliet, IL 60436, USA) and total organic carbon (TOC) by thermic combustion using an element analyzer, Euro 3000 (HEKAtech, Wegberg, Germany).

**Lithology and magnetic susceptibility.** The cores were cut longitudinally, photographed and analyzed for detailed lithology, using smear slides and measurements of magnetic susceptibility. The magnetic susceptibility was determined using a Bartington GT-2 surface probe (Bartington Instruments, Witney, Oxford, OX28 4GE, England) at intervals of 1 cm at cores that were cut open.[17,18]

**XRF core scanning.** A whole core of 35 cm length from site A was transported to Eawag, split in half along the length and opened. One half was used for a highly resolved and non-destructive determination of the Fe and Mn composition longitudinally using an Avaatech X-Ray Fluorescence (XRF) core scanner (Avaatech XRF, 1812 PS Alkmaar, Netherlands). The core was analyzed at 10 kV using steps of 2 and 5 mm, depending on the visually determined complexity of the sediment. The qualitative profile of Fe and Mn was subsequently calibrated according to the values from the ICP-MS analysis.

**Microbiology.** The other half of the opened core (see XRF core scanning) was sampled for microbial cell counting following Zarda *et al.*[19] Samples were taken from 35 different depths from the 35 cm long core and obtained by sectioning the core in 0.5 cm intervals with sterile metal disks and transferring each section into sterile 15 ml polypropylene tubes. Subsamples of 0.5 g of sediment were fixed overnight in 4% paraformaldehyde in phosphate buffered saline (PBS) at 4 °C. Fixed samples were washed twice with PBS and stored in 1 : 1 ethanol–PBS at −20 °C until analysis. Samples were stained with 4′,6-diamidino-2-phenylindole (DAPI) and analyzed following established protocols.[19] Stained cells were counted on 24 fields from two independently spotted wells per sample using a Zeiss Axioscope 2 epifluorescence microscope (Carl Zeiss AG, Oberkochen, Germany).

**Flux calculations.** Areal porewater fluxes ($J_{sed}$) were determined from concentration gradients applying Fick's first law of diffusion *e.g.* ref. 20.

$$J_{sed} = \phi D_{sed} \frac{dC}{dx}$$

$$D_{sed} = \frac{D_0}{\phi F}$$

Molecular diffusion coefficients ($D_0$) at 4 °C were taken from Li & Gregory.[21] $D_{sed}$ was calculated using the porosity $\phi$ and the formation factor $F$ as suggested by Maerki *et al.*[22]

$$F = 1.02\phi^{-1.81}$$

# 3 Results and discussion

## 3.1 Formation, transformation, and dissolution of Fe/Mn layers

The characteristic pattern of black layers of Mn oxides overlying thin layers of ochre colored Fe oxides in the top few centimeters of the sediment is widespread in Lake Baikal sediments and the occurrence of two or more layers is frequently observed.[7,8,23] Two principal types of layers could be distinguished in cores from sites A and B depicted in Fig. 2 and 3. As demonstrated by Och *et al.*,[12] the uppermost Fe/Mn enriched layer is commonly located right below the $O_2$ penetration depth, *i.e.* the $O_2$–Mn(II) redox interface, followed by Fe/Mn layers buried in the deeper, reducing parts of the sediments.

**3.1.1 Core description.** The data of cores from site A are given in Fig. 2. Five apparent peaks of particulate Mn are clearly distinguishable from the background content of 0.1%. While the uppermost accumulation is minor (Peak # 1), the highest two are found within a short interval between 5.5 and 8 cm depths within the Mn-reducing part of the sediment (Peaks # 2 and # 3) and two additional maxima occur at 13 cm and 18.5 cm (Peaks # 4 and # 5) depths. Accumulations of particulate Fe are observed at the same sediment depths as the Mn peaks, or slightly below (Peaks # 1 and # 2). The background concentration of particulate Fe, predominantly Fe oxides,[12] is about 4%. The porewater Mn(II) concentration increases from below detection limit underneath the uppermost Mn oxide layer, peaks around the maximum particulate Mn accumulations and decreases towards Peak # 4 at around 14 cm depth. Concentrations of dissolved Fe(II) are mostly below the measurable concentration range down to 9 cm depth with an exception at 4.5 cm, where an isolated peak of 7.5 μmol $l^{-1}$ occurs. Below 9 cm, between two Fe oxide peaks, a steep increase is observed, culminating to a maximum of 51 μmol $l^{-1}$ at a depth of 11 cm before steeply decreasing again down to ~15 μmol $l^{-1}$.

The data of cores from site B are given in Fig. 3. The particulate Mn content in the top layer was high (2.3%) and formed a peak (# 1) of up to 3.5% at 2.25 cm depth. Below 3 cm depth, a sharp decrease to background concentrations of around 0.1% is observed above a second peak (# 2) of 0.82% occurring at 10.25 cm depth. Like in core A, background contents of the particulate Fe were around 4%. Two major peaks were observed, where the first reached 6.3% right underneath the upper particulate Mn peak at 2.75 cm depth (Peak # 1), and the second reached 9.8% at the same depth as the lower particulate Mn peak (# 2). A slight increase in the Fe content occurred at a depth of around 14 cm (Peak # 3).

Porewater Mn(II) is first detected at 1.25 cm sediment depth. The concentration increases sharply to 41 μmol $l^{-1}$ at 2 cm

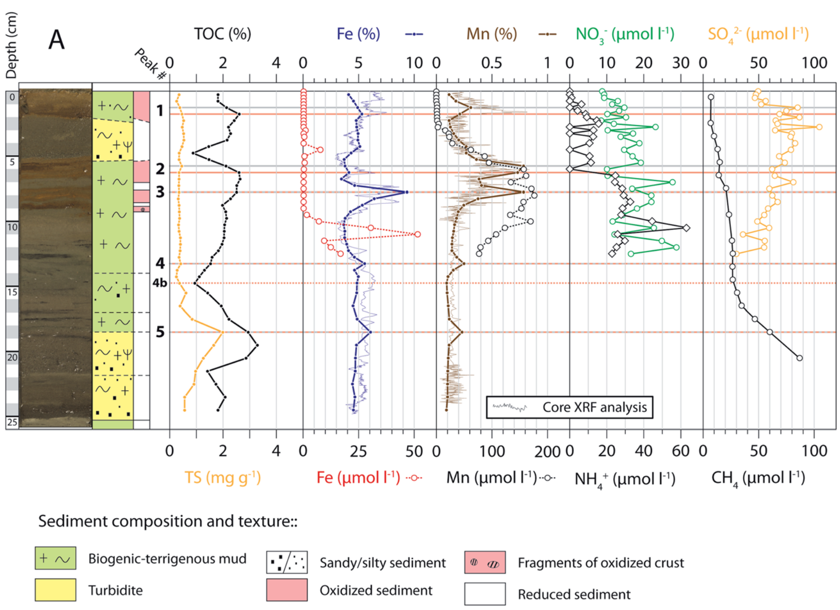


Fig. 2 Core A, its lithology, composition, and the geochemical profiles as discussed in the present study. Fe and Mn oxide enrichments discussed in the text are numbered (#).

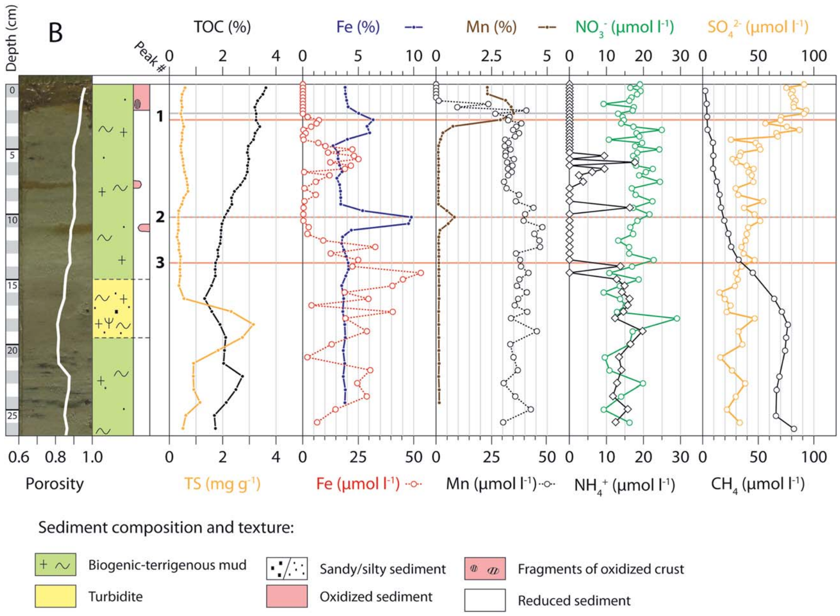


Fig. 3 Core B, its lithology, composition, and the geochemical profiles as discussed in the present study. Fe and Mn oxide enrichments discussed in the text are numbered (#).

depth and remains relatively constant at 30–48 µmol l$^{-1}$ for the remaining part of the analyzed core. Porewater Fe(II) always increased right below the Fe oxide accumulations. The concentration varies around a maximum of 7.2 µmol l$^{-1}$ at ~5.75 cm and a maximum of 53 µmol l$^{-1}$ at ~14.5 cm.

**3.1.2 Formation and transformation of the upper Fe/Mn layer.** The observation of similar multiple Fe/Mn layers in the uppermost ~50 cm of the sediments is rather exceptional and has so far been described not only from equatorial upwelling systems in the Atlantic and Pacific Oceans *e.g.* ref. 24 and the Centrals Arctic Ocean *e.g.* ref. 25–27, where they have been linked to climate variability, but also in lacustrine and marine environments such as in some settings of the Great Lakes[28,29] and Loch Lomond in Scotland.[30]

The low primary productivity[5] and efficient deep water mixing[31] of Lake Baikal ensure permanently oxygenated bottom water and an exceptionally high $O_2$ penetration depth.[6] Therefore, all the settling manganese and iron have been trapped within the sediments since the formation of Lake Baikal, and reductive dissolution sets in only several centimeters below the sediment surface. This situation is like that of the Central Arctic Ocean, which has been a low-productivity and well-ventilated setting through most of the quaternary, with deep $O_2$ penetration depths, and trapping of almost all settling Fe/Mn oxides within the deep basins.[32]

Due to the low sedimentation rates of 0.4–0.8 mm a$^{-1}$ in the south basin[12,33] and the high $O_2$ penetration depth, Mn(II) and Fe(II) from the reductive dissolution of their respective oxides diffuse upwards from the deeper sediment and are re-oxidized to Mn(IV) and Fe(III) accumulating as soon as porewaters contain appreciable $O_2$ concentrations again. The upper Fe/Mn accumulation (Peak # 1 in Fig. 2 and 3) is located at the active redox interface where upward diffusing Mn(II) is oxidized. Och *et al.*[12] have shown that $O_2$ penetrates the sediment surface down to the uppermost Mn oxide layer, which is located at 1 cm in core A and 1.25 cm in core B. In both cores the Fe layer as well as the peak of dissolved Fe(II) are positioned a few millimeters below the Mn layer, indicating that dissolved iron is oxidized in contact with Mn(IV), a fast abiotic reaction.[34,35] Thus, reducing conditions at the lower end of the Fe/Mn layer and oxidizing conditions on top (which is $O_2$ for Mn(II), and Mn(IV) for Fe(II)) allow for a dynamic adjustment of the solid phase Fe/Mn layer to the upward-moving redox interface of the accumulating sediment.

While the concentration profiles of particulate Fe and Mn as well as porewater Mn(II) of our cores are quite comparable with previous studies of Granina *et al.*[7] and Och *et al.*,[12] the Fe(II) profiles are markedly different, in particular within the upper oxic interval of the cores. Indeed, the presence of dissolved Fe in the uppermost oxic sediment layers as reported by Granina *et al.*[7] (Fig. 5b/d) and Och *et al.*[12] (Fig. 2 and 3) cannot, according to thermodynamic considerations, be Fe(II). Our measurements confirm previous arguments that a significant portion of Fe measured by ICP-MS after filtration through a 0.45 µm membrane and acidification with 5 µl $HNO_3$ can be attributed to colloidal iron.[36] The CE technique applied for porewater analyses in the present study guarantees the specific detection of dissolved Fe(II) *e.g.* ref. 37. Fig. 2 and 3 show that reduced Fe(II) in cores A and B was detected right below the top Mn layers and, thus, the upper limit of the iron reduction zone can be determined precisely with this analytical approach.

We expect that porewater profiles experience no significant influence from the inter-annual variability of physical parameters in Lake Baikal. First, because sedimentation rates are very low and predominantly originate from autochthonous deposition and second, seasonal convective mixing of the water column does not reach beneath 300 m depth.[31,38] There are, however, diatom blooms which occur every 3 to 5 years in spring which can influence porewater profiles in shallow sediment depths over short periods of time.[5]

**3.1.3 Dissolution of buried Fe/Mn layers.** Both cores contain one or more Fe/Mn oxide layers (Peak # 2 in Fig. 2, Peaks # 2 and 3 in Fig. 3) buried in the reducing sediment, *i.e.* below the upper dynamic Fe/Mn oxide layers. Such buried layers have even been found in the Baikal sediment up to 65 000–85 000 years old[3] and, as is apparent from the porewater profiles of Fe(II), Mn(II), phosphate and other compounds[11] dissolve slowly, thereby providing additional Fe and Mn to younger sediment layers. The TOC content in Lake Baikal sediments is rather high throughout the cores (between 1 and 3% in core A and 1–3.6% in core B), suggesting that the organic carbon is, to a certain degree, refractory with a diminished electron donor capacity. This is particularly evident since sedimentation rates are low, notably around 0.4 mm in this area of the lake,[33] meaning that the turbidites below Peak # 5 in core A and Peak # 3 in core B result from 500 and 400 year old events respectively. The highly variable TOC profile in core A likely results from the numerous turbiditic depositions and is not directly correlated with the Fe/Mn oxide enrichments. Nonetheless, substantial $CH_4$ fluxes from the deeper sediment indicate that organic matter degradation remains an important driving force for early diagenesis but it is likely that $CH_4$ is the key electron donor in this system. Thus, considering $CH_4$ as the ultimate electron donor, we will discuss the sequence of redox reactions starting from the bottom of the analyzed cores. In each core, $CH_4$ is predominantly consumed within short intervals close to the occurrence of buried Fe (and Mn) oxides, *e.g.* at 16.5 cm depth in core A and 13 cm depth in core B. $CH_4$ can be oxidized not only anaerobically (AOM) by sulphate,[39,40] but potentially also by Fe and Mn oxides[41] and $NO_3^-$.[42] These methane oxidation processes can thus contribute to the production of reduced species such as S(−II), Fe(II), Mn(II), and $NH_4^+$.

The Fe(II) released from the deepest layers diffuses to the overlying Mn(IV) layer and is oxidized, thus releasing Mn(II),[35] as can be seen in Fig. 2 (Peak # 2).

The present data do not allow deciding whether $CH_4$ is oxidized by sulphate or rather by Fe oxides. While there might be a clarifying intersection between the $CH_4$ and $SO_4^{2-}$ profiles in core A if the downward trend in $SO_4^{2-}$ concentrations is extrapolated linearly, indicating AOM by sulphate, we do not see a significant effect in the $SO_4^{2-}$ profile of core B. If $CH_4$ was oxidized by $SO_4^{2-}$, we would postulate a cryptic sulphur cycle, where produced S(−II) is recycled to $S^0$ in contact with Fe(III) oxides.[43–45] It has been shown, however, that further oxidation of $S^0$ by Fe(III) is inefficient as opposed to oxidation by Mn(IV).[46–49] Hence, if Fe oxides were directly reduced by $CH_4$, 8 moles $Fe^{2+}$ must be released for every mole of oxidized $CH_4$:[41]

$$CH_4 + 8Fe(OH)_3 + 15H^+ \rightarrow HCO_3^- + 8Fe^{2+} + 21H_2O \quad (1)$$

However, if $SO_4^{2-}$ was reduced by $CH_4$ prior to the reductive dissolution of Fe oxides by the resulting sulphides, only 2 moles of Fe(II) are generated by the oxidation of 1 mole $CH_4$ according to:

$$CH_4 + SO_4^{2-} \rightarrow HCO_3^- + HS^- + H_2O \quad (2)$$

$$2FeOOH + HS^- + 5H^+ \rightarrow 2Fe^{2+} + S^0 + 4H_2O \quad (3)$$

A constant supply of $SO_4^{2-}$ is indicated around the buried Fe/Mn accumulation in most Lake Baikal surface sediments (due to a cryptic sulphur cycle[12]). Hence, the oxidation of $S^0$ is likely to involve either Mn(IV) oxides[47] or other microbial pathways, such as through *Thioploca* spp. or through disproportionating bacteria from sulphur intermediates.[49] Considering a pathway involving the oxidation of $S^0$ by Mn(IV)[47] the resulting reaction can be summarized as:

$$CH_4 + 2FeOOH + 3MnO_2 + 9H^+ \rightarrow HCO_3^- + 2Fe^{2+} + 3Mn^{2+} + 7H_2O \quad (4)$$

As the reaction is faster than the diffusion of $CH_4$, only small amounts of $SO_4^{2-}$ may be required to keep up the transfer of electrons from $CH_4$ to Fe(III) and may not cause detectable effects in the $SO_4^{2-}$ concentration profile. In order to test whether the above considerations make sense stoichiometrically, we performed diffusive flux calculations using porewater Mn(II), Fe(II) and $CH_4$ profiles.

It is more suitable to start with core B as the porewater profiles extend down to greater depth and are more suitable to illustrate our case. There, the upward methane flux towards Peak # 3 in Fig. 3 is $\sim$15 mmol $m^{-2}$ $a^{-1}$. Assuming that the AOM involving Fe oxides lead to the release of Fe(II) without the formation of solid phases or consumption by $MnO_2$, we expect an either eightfold (reaction (1)) or a twofold (reaction (4)) higher flux of Fe(II), *i.e.* $\sim$120 mmol $m^{-2}$ $a^{-1}$ Fe(II) or $\sim$30 mmol $m^{-2}$ $a^{-1}$ Fe(II). Although the Fe(II) concentrations were very variable across the core, we can evaluate the flux according to a more schematic profile characterized as a succession of peaks with amplitudes increasing with depth. As a result, the dissolution rate of Fe oxides at Peak # 3 is at least 20 mmol $m^{-2}$ $a^{-1}$. However, if the interval taken for the calculation of the fluxes is reduced to the immediate vicinity of Peak # 3 (Fig. 3), *i.e.* between 13 and 16 cm depths, the dissolution rate of Fe oxides increases to 50 mmol $m^{-2}$ $a^{-1}$. Hence, observed Fe oxide dissolution rates are between 20 and 50 mmol $m^{-2}$ $a^{-1}$ and thus support a pathway where AOM proceeds through the reduction of sulphate and only indirectly through the reductive dissolution of Fe oxides. However, although reactive Mn oxides are present close to Peak # 3, the precise pathways leading to the formation of $SO_4^{2-}$ are currently not conclusive.

Similarly in core A the $CH_4$ flux towards the Fe oxide Peak # 4 and/or 4b in Fig. 2 was >25 mmol $m^{-2}$ $a^{-1}$ and could therefore release a maximum of $\sim$200 mmol $m^{-2}$ $a^{-1}$ Fe(II) (reaction (1)) or $\sim$50 mmol $m^{-2}$ $a^{-1}$ (reaction (4)), respectively. Unfortunately there are not enough porewater data to calculate meaningful Fe oxide dissolution rates but the presence of such small Fe oxide accumulations as in Peaks # 4, 4b and 5 would be highly unlikely if the AOM would directly reduce Fe oxides rather than sulphate. Hence, we suggest that the pattern in core A also points toward the oxidation of $CH_4$ by sulphate and subsequent formation of elemental S by the reduction of Fe(III).

### 3.2 Redox discontinuity caused by the Fe/Mn layers

The incidental burials of oxidized layers of Fe and Mn in the methanogenic sediment introduce zones of slowly reacting electron acceptors with a large capacity. Thus, the continuous succession of redox reactions usually observed in sediments allowing for a steady-state situation between provision of organic matter at the sediment surface and a subsequent degradation by the typical cascade of electron acceptors at depth, as sketched *e.g.* by Froelich *et al.*,[10] does not hold for Lake Baikal sediments. The oxidized zones of the slowly reacting Fe/Mn phases embedded in a reducing environment cause complex interactions in the vertical diagenetic profile.

Vertical heterogeneity caused by short-term sedimentary events disrupts steady-state processes and might temporarily stimulate microbial growth.[50–52] The microbial distribution across core A (Fig. 4) reflects the overall heterogenetic character of Lake Baikal sediments.

Interestingly, peaks in the cell counts coincide with peaks of Mn(IV) and in particular Fe(III) enrichments, prompting the conclusion that the biogeochemical cycling of Mn and Fe shaped the microbial communities in the surface sediments of Lake Baikal. Hence, early assumptions can be made regarding the dominant microbial pathways involved in the Fe and Mn cycling: (1) the uppermost 2 cm may harbor Mn oxidizing (aerobic) microbes while the underlying 2 cm are likely to be dominated by Fe oxidizing microbial pathways coupled to organic matter degradation. (2) Although a large cell peak is observed within the layer of maximum Mn enrichment, the highest cell counts correlate better with smaller peaks in the Fe content and therefore might indicate microbial pathways that reductively dissolve Mn oxide by Fe(II). (3) Below 10 cm, the microbial abundance is rather low but increases again at the next buried oxide layer between 23 and 26 cm, possibly reflecting the presence of a microbial community based on methanotrophy. Further studies into the phylogenetic and functional composition on the microbial community would be required to test these hypotheses.

**3.2.1 Anaerobic nitrification by Mn oxides.** Porewater nitrate was observed throughout all investigated cores in concentrations of 10–20 μmol $l^{-1}$. These concentrations were higher than in the overlying water (~10 μmol $l^{-1}$) and could therefore not be caused by diffusion through the sediment–water interface but must originate from anaerobic nitrification in the sediment. Two questions arise in this context: first, what is the oxidant that causes nitrification in the anaerobic sediment, and second, why does $NO_3^-$ persist in the porewater and is it not denitrified by the available reductants?

The $NH_4^+$ porewater profiles (Fig. 2 and 3) are unsteady in both sediment cores. In homogeneous sediments, a smooth increase in the concentration of $NH_4^+$ with depth is usually observed, as it is the degradation product of amino acids in an anoxic environment. However, $NH_4^+$ can be re-assimilated into biomass or sorb onto clay minerals and/or re-oxidized to nitrite or nitrate during nitrification or anaerobic ammonium oxidation *e.g.* ref. 53–57.

In core A (see Fig. 2), $NH_4^+$ is already detected at 0.5 cm depth, followed by a two-step increase, initially to 10–15 μmol $l^{-1}$ at 1 cm and, after a few incidental excursions back to zero, to ~30 μmol $l^{-1}$ at 6.5 cm. Both steps are delimited by Fe/Mn oxide layers (Peaks # 1 and 2). A single $NH_4^+$ peak of up to 64 μmol $l^{-1}$ occurs between Peaks # 3 and 4.

In core B (see Fig. 3), $NH_4^+$ is first detected at 5.5 cm (between Peaks # 1 and 2) before concentrations increase to 18 μmol $l^{-1}$ with zones devoid of $NH_4^+$ between Peaks # 2 and 3. Steady concentrations of ~15 μmol $l^{-1}$ prevail below 14 cm depth underneath Peak # 3.

Nitrate and ammonium anomalies were found in several other studies and sometimes explained as sampling artefacts due to cell bursting during centrifugation, stress reactions of the sediment fauna during decompression, and warming of the

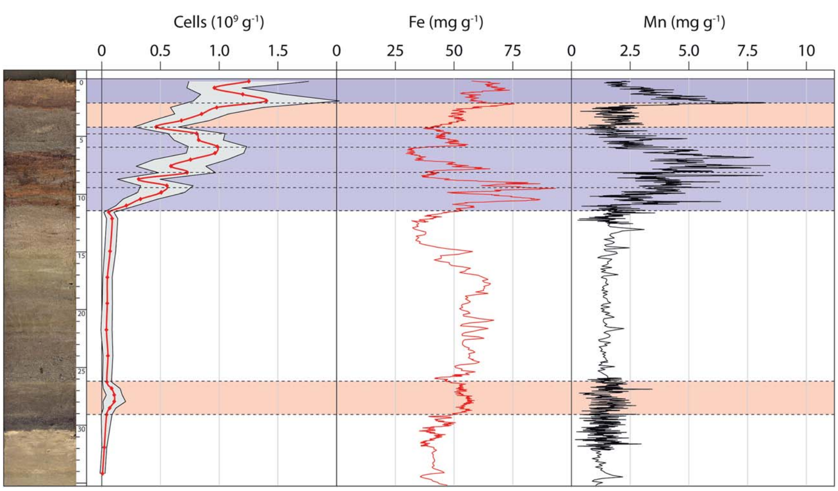


Fig. 4 Depth profile of DAPI-stained cells in the sediment (with standard deviation in grey). The core was taken close to the location of core A. Peaks at 2, 6, 9.5 and 28 cm depth confirm the heterogeneity of the sediment. The peaks coincide clearly with the visible Mn oxide (blackish) and Fe oxide (reddish) layers from the photograph as well as with the XRF scan reflecting Mn and Fe oxide levels. The top peak at 2 cm corresponds to the current oxic–anoxic interface.

sediment core *e.g.* ref. 58 and 59. We also found discontinuous $NH_4^+$ porewater profiles and the occurrence of $NO_3^-$ in anoxic sediment strata in data from previous field trips to Lake Baikal throughout all porewater measurements using various methods for sampling as well as for analyses (B. Müller, unpublished data). Furthermore, we observed a close correlation between the vertical concentration patterns of $NO_3^-$ and $SO_4^{2-}$ but not with $Cl^-$ (data not shown). Hence, we exclude a bias in the analytical determination of anions by CE. So far, it was unclear whether the exceptional $NH_4^+$ and $NO_3^-$ concentration profiles represented the true situation or were caused by unknown bias. The results of the on-site measurements in this study, designed to avoid such sampling artefacts, confirmed the previous findings. Due to the irregular occurrence of buried oxidized Fe/Mn layers in the Baikal sediments, the redox sequence is discontinuous, and we do not have a successively increasing reductive intensity with depth. The intermittently distributed oxides of Mn(IV) (and potentially Fe(III)) can act as oxidants for microbially mediated nitrification, which was observed by Luther *et al.*,[60] Aller *et al.*,[61] as well as Anschutz *et al.*,[62] and investigated by Hulth *et al.*[55] and Bartlett *et al.*[53] Anomalies of N species in marine sediments were also observed by several other authors[50,58,63] and more recently also in a lacustrine system.[64] The direct oxidation to $N_2$ or the oxidation to $NO_3^-/NO_2^-$ and subsequent denitrification are possible. The following equation for anaerobic nitrification was proposed by Hulth *et al.*:[55]

$$4MnO_2 + NH_4^+ + 6H^+ \rightarrow 4Mn^{2+} + NO_3^- + 5H_2O \qquad (5)$$

However, there have been difficulties in obtaining conclusive evidence for the anaerobic oxidation of ammonium by Mn oxides.[65,66] Bartlett *et al.*[53] put forward that sediment perturbations might be a prerequisite for the expression of anaerobic nitrification (reaction (5)), be it physical or chemical. The otherwise unusual presence of large amounts of Mn oxides buried in Lake Baikal sediments is likely to represent such a case. Similarly, anaerobic nitrification might occur in the presence of Fe(III)oxides. However, Anschutz *et al.*[50] estimated that this pathway was feasible only when Fe(II) concentrations were low and pH relatively high. Hence, the nitrification of $NH_4^+$ by Fe oxides was considered less likely than by Mn oxides. A close coupling of reaction (5) with the sulphur cycle is suggested, as the profiles of $NO_3^-$ and $SO_4^{2-}$ often covary (see Fig. 2 and 3), which could be explained by the biogenic oxidation of labile sulphides:[46]

$$4\,MnO_2 + 8H^+ + FeS(s) \rightarrow 4Mn^{2+} + SO_4^{2-} + Fe^{2+} + 4H_2O \qquad (6)$$

The simultaneous oxidation of labile S(−II) (and possibly S(0)) and $NH_4^+$ with reactive $MnO_2$ particulate surfaces could explain the correlated pattern of $NO_3^-$ and $SO_4^{2-}$ porewater concentrations. However, the unusually high $NO_3^-$ and $SO_4^{2-}$ concentrations reaching deeply into the sediments deserve further considerations and we outline possible processes in the following section.

**3.2.2 Nitrate and sulphate anomalies.** While the profiles of most species adequately reflect the dominant early diagenetic processes in the surface sediments of Lake Baikal, the detection of $NO_3^-$ and $SO_4^{2-}$ in the methanogenic sediment zones of both cores represent the most unusual result encountered in the present study.

In core A (Fig. 2), $NO_3^-$ concentrations slightly increase with depth and exhibit considerable variations, from 8 μmol $l^{-1}$ at the sediment water interface to 29 μmol $l^{-1}$ at depth. $SO_4^{2-}$ first reaches concentrations of up to 104 μmol $l^{-1}$ at 2.75 cm depth, which is even higher than in the overlying water (49 μmol $l^{-1}$) and then slowly decreases down to 30 μmol $l^{-1}$.

$NO_3^-$ concentrations in core B (Fig. 3) remain within the same range as in core A with an average of 17 μmol $l^{-1}$ (16 μmol $l^{-1}$ in core A), a minimum of 9 and a maximum of 29 μmol $l^{-1}$. The $SO_4^{2-}$ concentrations are up to 90 μmol $l^{-1}$ within the uppermost sediment and decrease down to 50 μmol $l^{-1}$ at a depth of about 4.5 cm. The concentrations remain generally above 20 μmol $l^{-1}$ until the end of the core at 26 cm, but exhibit a sharp decrease underneath the upper Fe and Mn oxide accumulation (Peak # 1) before aligning with $NO_3^-$. In the previous chapter we discussed biogeochemical reactions that explained the occurrence of these oxidized species in a heterogeneous sediment. However, it is more puzzling how these species could be preserved in sediment where potential reductants such as Mn(II), Fe(II), TOC, and $CH_4$ are abundant. However, similar concentration profiles were previously observed in Lake Baikal sediments[67,68] (Müller, unpublished data) as well as in other lacustrine[64] and marine surface sediments.[50,63,69]

We calculated the thermodynamic equilibrium for the prevailing chemical conditions of the sediment and found that denitrification by Mn(II) can be ruled out, which is in agreement with the estimations of Hulth *et al.*[55] Testing Fe(II) as a possible reductant for $NO_3^-$ (ref. 70) revealed that the sediment was approximately at equilibrium with the prevailing concentrations, pH 6 and a $pN_2$ of 1 atm. TOC, in spite of the high sediment content, was already ruled out as a significant reductant for the buried Fe/Mn layers and, apparently, did not affect $NO_3^-$ concentrations in the porewater during the observed time scale (sediment depth) either. It seems that the reactivity of the buried TOC, probably due to its long exposure to oxic conditions, is very low and only slow fermentation at greater depth, *i.e.* a longer time scale, eventually leads to the formation of $CH_4$. Thus, only $CH_4$ remains as an unambiguous potential reductant for $NO_3^-$, at least in thermodynamic terms. Until the recent discovery of a microbial consortium[71,72] that actually linked AOM to denitrification[42] there was no experimental evidence of this reaction and the pathway was considered "missing in nature". Apparently, these microorganisms develop with a very slow growth rate only in the total absence of other oxidants. This may be a reason why this oxidation pathway had never been observed in lacustrine or marine sediments before, and in Lake Baikal it would have to occur at lower rates than the production of nitrate. Considering all the above arguments, we can thus explain the formation and the persistence of $NO_3^-$ in the sediment porewater. Explaining the presence of $SO_4^{2-}$, however, is more challenging.

The possibility of a cryptic sulphur cycle deeper in the sediment has already been mentioned in Section 3.1.3 but, unlike previous studies on Lake Baikal sediment porewaters,[12] elevated $SO_4^{2-}$ concentrations are not limited to the intervals with large Fe and Mn oxide enrichments and other microbial pathways should also be considered. Several authors reported the presence of vertically migrating facultative chemoautotrophic sulphide-oxidizing bacteria, *Thioploca* spp. in marine[73–75] and lacustrine environments[76–78] and in Lake Baikal.[68,79,80] They are phylogenetically similar to *Beggiatoa* spp. and are able to pump $NO_3^-$ from the bottom water into the sediment. $NO_3^-$ is accumulated intracellularly to concentrations up to four orders of magnitude higher than bottom-water concentrations.[73] Within their sheaths they can vertically glide down over 15 cm and reduce $NO_3^-$ to $NH_4^+$ and $NO_2^-$, concomitant with the oxidation of S(−II), which provides perfect conditions for anammox bacteria too.[81] Interestingly, Zemskaya *et al.*[68] found increased $SO_4^{2-}$ (up to 800 μmol $l^{-1}$) and $NO_3^-$ (20–500 μmol $l^{-1}$) concentrations in some *Thioploca* habitats in Lake Baikal sediments. Although we did not find any visual evidence of *Thioploca* filaments in our cores, their potential existence cannot currently be excluded. To obtain further information on the presence of *Thioploca* spp. or *Beggiatoa* spp., we plan to extract the DNA from Lake Baikal sediments and analyze the microbial community composition in a next step.

### 3.3 Burial of the Fe/Mn layers

Vertical profiles of element contents and porewater fluxes in the sediments allow conclusions on the biogeochemical processes controlling the formation and transformation of Fe/Mn layers right below the $O_2$–Mn(II) redox interface and the gradual dissolution of buried layers in the reducing (methanogenic) sediment. However, the critical incident required to bury a Fe/Mn layer in the sediment cannot, at present, be investigated by measurements. Four scenarios affecting the position of the $O_2$–Mn(II) redox interface may be anticipated:

• Changes in the mass accumulation rate of organic matter: an increase of the settling organic matter would increase the sediment oxygen consumption and thus $O_2$ penetration depth.

• Decreasing bottom water $O_2$ concentration due to restrained water column mixing would decrease $O_2$ penetration.

• A growing Fe/Mn layer could at some point constrain the diffusion of dissolved compounds.

• The increasing sedimentation rate would enlarge the diffusive pathway and separate the $O_2$–Mn(II) interface.

The first two processes might result from climatic variations over the last 1000 years *e.g.* ref. 82, but it is difficult to infer that from the geochemical profiles alone. The third process is unlikely as the diffusivity across the Fe/Mn oxide accumulations is only marginally slower considering the range of calculated porosities in the present study. However, the last process could be confirmed from the lithology of core A, which incidentally shows the occurrence of a turbidite layer of 3 cm magnitude about 0.5 cm right above a Fe/Mn layer (Fig. 5).

Sediment slides, however, are not a frequent cause for the detachment of Fe/Mn layers and we have never observed them above buried Fe/Mn oxide enrichments in other sediment cores from Lake Baikal. To date, none of the other processes

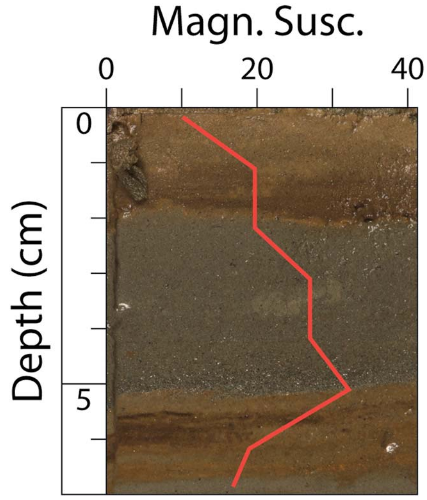


Fig. 5 A turbiditic sediment layer (core A: 2–5 cm depth), clearly visible in the photo and indicated by higher magnetic susceptibility (red line), is overlaying the uppermost buried Fe/Mn layer (below 5 cm).

suggested above could be evidenced with sediment analyses. Currently, we apply a diagenetic computer model to estimate the constraining variables for the formation, detachment and dissolution of Fe/Mn layers (Och *et al.*, in preparation).

## 4 Conclusions

One of the unique features in the Lake Baikal sediments is the redox heterogeneity introduced by the temporally irregular detachment of oxidized layers of Mn and Fe. The occurrence of the resulting sediment structures is rare in such clear patterns, thus allowing the investigation of distinct diagenetic processes and rates. These are mirrored in the porewater samples where the investigation requires advanced analytical equipment to meet the demands of fast sampling, of small volumes, and on-site treatment and analyses.

The application of Rhizon porewater samplers in combination with portable CE instruments with a contact-free detector cell proved to be ideal and reliable for fieldwork even when local working conditions were challenging. Using the resulting porewater data we were able to explain the geochemical reactions leading to the formation and reductive dissolution of Fe/Mn layers and discuss the consequences of diagenetic processes that cause non-steady-state sediment patterns. Concerns about the quality of earlier data from samples of $NH_4^+$, $NO_3^-$ and $SO_4^{2-}$, that were hypothesized to change during sampling in Siberia, transportation to and analyses in Switzerland, have been dispelled. Further investigations will be required to fully understand the causes of the presence of $SO_4^{2-}$ in the methanogenic porewater.

## Acknowledgements

We are indebted to Professor Nikolay M. Budnev (State University Irkutsk) and Professor Eugene V. Sklyarov (RAS-SB Institute of Earth Crust, Irkutsk) for their support during fieldwork at Lake Baikal. The authors would like to thank Ursula Brupbacher (ETH Zurich) for the XRF analyses, Serge Robert for the methane analyses, Irène Brunner for TOC and TIC determination, Patrick Kathriner for the water content measurements, David Kistler and Claudio Steger for the metal analyses, Karin Beck for the microbial counts, Beat Kienholz for the core photograph and Michael Schurter for organizing the trip. The project was made possible by the Swiss National Science Foundation (Grant no. 200021-137715).

## References

1 V. D. Mats and T. I. Perepelova, *Geosci. Front.*, 2011, **2**, 349–365.
2 D. F. Williams, J. Peck, E. B. Karabanov, A. A. Prokopenko, V. Kravchinsky, J. King and M. I. Kuzmin, *Science*, 1997, **278**, 1114–1117.
3 R. G. Deike, L. Granina, E. Callender and J. J. McGee, *Mar. Geol.*, 1997, **139**, 21–46.
4 T. Sapota, A. Aldahan and I. Al-Aasm, *J. Paleolimnol.*, 2006, **36**, 245–257.
5 B. Müller, M. Maerki, M. Schmid, E. G. Vologina, B. Wehrli, A. Wüest and M. Sturm, *Global Planet. Change*, 2005, **46**, 101–124.
6 P. Martin, L. Granina, K. Martens and B. Goddeeris, *Hydrobiologia*, 1998, **367**, 163–174.
7 L. Granina, B. Müller and B. Wehrli, *Chem. Geol.*, 2004, **205**, 55–72.
8 L. Granina, E. Karabanov and E. Callender, *IPPCCE Newslett.*, 1993, **7**, 32–39.
9 V. D. Mats, O. M. Khlystov, M. De Batist, S. Ceramicola, T. K. Lomonosova and A. Klimansky, *Int. J. Earth Sci.*, 2000, **89**, 229–250.
10 P. N. Froelich, G. P. Klinkhammer, M. L. Bender, N. A. Luedtke, G. R. Heath, D. Cullen, P. Dauphin, D. Hammond, B. Hartman and V. Maynard, *Geochim. Cosmochim. Acta*, 1979, **43**, 1075–1090.
11 B. Müller, L. Granina, T. Schaller, A. Ulrich and B. Wehrli, *Environ. Sci. Technol.*, 2002, **36**, 411–420.
12 L. M. Och, B. Müller, A. Voegelin, A. Ulrich, J. Göttlicher, R. Steiniger, S. Mangold, E. G. Vologina and M. Sturm, *Chem. Geol.*, 2012, **330–331**, 244–259.
13 N. T. Torres, P. C. Hauser, G. Furrer, H. Brandl and B. Müller, *Environ. Sci.: Processes Impacts*, 2013, **15**, 715–720.
14 A. M. Shiller and E. Boyle, *Nature*, 1985, **317**, 49–52.
15 P. Kuban, H. T. A. Nguyen, M. Macka, P. R. Haddad and P. C. Hauser, *Electroanalysis*, 2007, **19**, 2059–2065.
16 R. W. Sterner and J. J. Elser, *Ecological Stoichiometry: The Biology of Elements from Molecules to the Biosphere*, Princeton University Press, 2002.
17 E. G. Vologina, M. Sturm, Y. B. Radziminovich, S. S. Vorob'eva and A. A. Shchetnikov, *Russ. Geol. Geophys.*, 2012, **53**, 1342–1350.
18 N. R. Urban, K. Ernst and S. Bernasconi, *Geochim. Cosmochim. Acta*, 1999, **63**, 837–853.
19 B. Zarda, D. Hahn, A. Chatzinotas, W. Schönhuber, A. Neef, R. I. Amann and J. Zeyer, *Arch. Microbiol.*, 1997, **168**, 185–192.
20 R. A. Berner, *Early diagenesis: a theoretical approach*, Princeton University Press, 1980.
21 Y.-H. Li and S. Gregory, *Geochim. Cosmochim. Acta*, 1974, **38**, 703–714.
22 M. Maerki, B. Wehrli, C. Dinkel and B. Müller, *Geochim. Cosmochim. Acta*, 2004, **68**, 1519–1528.
23 E. G. Vologina, M. Sturm, S. S. Vorob'eva, L. Z. Granina and S. Y. Toshchakov, *Russ. Geol. Geophys.*, 2003, **44**, 407–421.
24 D. J. Burdige, *Earth-Sci. Rev.*, 1993, **35**, 249–284.
25 C. März, A. Stratmann, J. Matthiessen, A. K. Meinhardt, S. Eckert, B. Schnetger, C. Vogt, R. Stein and H. J. Brumsack, *Geochim. Cosmochim. Acta*, 2011, **75**, 7668–7687.
26 L. Löwemark, C. März, M. O'Regan and R. Gyllencreutz, *Quat. Sci. Rev.*, 2014, DOI: 10.1016/j.quascirev.2013.11.018.
27 L. Löwemark, M. O'Regan, T. J. J. Hanebuth and M. Jakobsson, *Palaeogeogr., Palaeoclimatol., Palaeoecol.*, 2012, **365–366**, 192–208.
28 R. Rossmann and E. Callender, *Science*, 1968, **162**, 1123–1124.
29 L. L. Richardson and K. H. Nealson, *J. Great Lakes Res.*, 1989, **15**, 123–132.
30 J. G. Farmer and M. A. Lovell, *Environ. Technol. Lett.*, 1984, **5**, 257–262.
31 M. Schmid, N. M. Budnev, N. G. Granin, M. Sturm, M. Schurter and A. Wüest, *Geophys. Res. Lett.*, 2008, **35**, L09605.
32 R. Macdonald and C. Gobeil, *Aquat. Geochem.*, 2012, **18**, 565–591.
33 U. Morgenstern, R. G. Ditchburn, E. G. Vologina and M. Sturm, *J. Paleolimnol.*, 2013, **50**, 345–352.
34 D. Postma, *Geochim. Cosmochim. Acta*, 1985, **49**, 1023–1033.
35 D. Postma and C. A. J. Appelo, *Geochim. Cosmochim. Acta*, 2000, **64**, 1237–1247.
36 J. Wu, E. Boyle, W. Sunda and L.-S. Wen, *Science*, 2001, **293**, 847–849.
37 J. R. Lead and K. J. Wilkinson, *Environ. Chem.*, 2006, **3**, 159–171.
38 R. F. Weiss, E. C. Carmack Carmack and V. M. Koropalov, *Nature*, 1991, **349**, 665–669.
39 K. Knittel and A. Boetius, *Annu. Rev. Microbiol.*, 2009, **63**, 311–334.
40 C. J. Schubert, F. Vazquez, T. Lösekann-Behrens, K. Knittel, M. Tonolla and A. Boetius, *FEMS Microbiol. Ecol.*, 2011, **76**, 26–38.
41 E. J. Beal, C. H. House and V. J. Orphan, *Science*, 2009, **325**, 184–187.
42 A. A. Raghoebarsing, A. Pol, K. T. van de Pas-Schoonen, A. J. P. Smolders, K. F. Ettwig, W. I. C. Rijpstra, S. Schouten, J. S. S. Damste, H. J. M. Op den Camp, M. S. M. Jetten and M. Strous, *Nature*, 2006, **440**, 918–921.
43 M. Dos Santos Afonso and W. Stumm, *Langmuir*, 1992, **8**, 1671–1675.
44 S. Peiffer, M. Dos Santos Afonso, B. Wehrli and R. Gaechter, *Environ. Sci. Technol.*, 1992, **26**, 2408–2413.
45 L. Holmkvist, T. G. Ferdelman and B. B. Jørgensen, *Geochim. Cosmochim. Acta*, 2011, **75**, 3581–3599.

46 R. C. Aller and P. D. Rude, *Geochim. Cosmochim. Acta*, 1988, **52**, 751–765.
47 D. R. Lovley and E. J. P. Phillips, *Appl. Environ. Microbiol.*, 1994, **60**, 2394–2399.
48 W. Yao and F. J. Millero, *Mar. Chem.*, 1996, **52**, 1–16.
49 J. Zopfi, M. E. Böttcher and B. B. Jørgensen, *Geochim. Cosmochim. Acta*, 2008, **72**, 827–843.
50 P. Anschutz, B. Sundby, L. Lefrançois, G. W. Luther Iii and A. Mucci, *Geochim. Cosmochim. Acta*, 2000, **64**, 2751–2763.
51 B. Deflandre, A. Mucci, J.-P. Gagné, C. Guignard and B. j. Sundby, *Geochim. Cosmochim. Acta*, 2002, **66**, 2547–2558.
52 F. C. Van Duyl, W. Van Raaphorst and A. J. Kop, *Mar. Ecol.: Prog. Ser.*, 1993, **100**, 85.
53 R. Bartlett, R. J. G. Mortimer and K. Morris, *Chem. Geol.*, 2008, **250**, 29–39.
54 J.-C. Clément, J. Shrestha, J. G. Ehrenfeld and P. R. Jaffé, *Soil Biol. Biochem.*, 2005, **37**, 2323–2328.
55 S. Hulth, R. C. Aller and F. Gilbert, *Geochim. Cosmochim. Acta*, 1999, **63**, 49–66.
56 J. E. Mackin and R. C. Aller, *Limnol. Oceanogr.*, 1984, **29**, 250–257.
57 B. Thamdrup and T. Dalsgaard, in *Microb. Ecol. Oceans*, John Wiley & Sons, Inc., 2008, pp. 527–568, DOI: 10.1002/9780470281840.ch14.
58 D. E. Hammond, J. McManus, W. M. Berelson, T. E. Kilgore and R. H. Pope, *Deep Sea Res., Part II*, 1996, **43**, 1365–1412.
59 W. B. Homoky, D. J. Hembury, L. E. Hepburn, R. A. Mills, P. J. Statham, G. R. Fones and M. R. Palmer, *Geochim. Cosmochim. Acta*, 2011, **75**, 5032–5048.
60 G. W. I. Luther, B. Sundby, B. L. Lewis, P. J. Brendel and N. Silverberg, *Geochim. Cosmochim. Acta*, 1997, **61**, 4043–4052.
61 R. C. Aller, P. O. J. Hall, P. D. Rude and J. Y. Aller, *Deep Sea Res., Part I*, 1998, **45**, 133–165.
62 P. Anschutz, K. Dedieu, F. Desmazes and G. Chaillou, *Chem. Geol.*, 2005, **218**, 265–279.
63 C. Hyacinthe, P. Anschutz, P. Carbonel, J. M. Jouanneau and F. J. Jorissen, *Mar. Geol.*, 2001, **177**, 111–128.
64 J. Tapia and S. Audry, *Appl. Geochem.*, 2013, **31**, 60–78.
65 R. Bartlett, R. J. G. Mortimer and K. M. Morris, *Cont. Shelf Res.*, 2007, **27**, 1501–1509.
66 B. Thamdrup and T. Dalsgaard, *Geochim. Cosmochim. Acta*, 2000, **64**, 4157–4164.
67 T. V. Pogodaeva, T. I. Zemskaya, L. P. Golobokova, O. M. Khlystov, H. Minami and H. Sakagami, *Russ. Geol. Geophys.*, 2007, **48**, 886–900.
68 T. I. Zemskaya, S. M. Chernitsyna, N. M. Dul'tseva, V. N. Sergeeva, T. V. Pogodaeva and B. B. Namsaraev, *Microbiology*, 2009, **78**, 117–124.
69 N. S. Suits and M. A. Arthur, *Deep Sea Res., Part I*, 2000, **47**, 1829–1853.
70 J. Sørensen, *Geomicrobiol. J.*, 1987, **5**, 401–421.
71 K. F. Ettwig, M. K. Butler, D. Le Paslier, E. Pelletier, S. Mangenot, M. M. M. Kuypers, F. Schreiber, B. E. Dutilh, J. Zedelius, D. de Beer, J. Gloerich, H. J. C. T. Wessels, T. van Alen, F. Luesken, M. L. Wu, K. T. van de Pas-Schoonen, H. J. M. Op den Camp, E. M. Janssen-Megens, K.-J. Francoijs, H. Stunnenberg, J. Weissenbach, M. S. M. Jetten and M. Strous, *Nature*, 2010, **464**, 543–548.
72 K. F. Ettwig, S. Shima, K. T. Van De Pas-Schoonen, J. Kahnt, M. H. Medema, H. J. M. Op Den Camp, M. S. M. Jetten and M. Strous, *Environ. Microbiol.*, 2008, **10**, 3164–3173.
73 H. Fossing, V. A. Gallardo, B. B. Jorgensen, M. Huttel, L. P. Nielsen, H. Schulz, D. E. Canfield, S. Forster, R. N. Glud, J. K. Gundersen, J. Kuver, N. B. Ramsing, A. Teske, B. Thamdrup and O. Ulloa, *Nature*, 1995, **374**, 713–715.
74 B. B. Jørgensen and V. A. Gallardo, *FEMS Microbiol. Ecol.*, 1999, **28**, 301–313.
75 B. Thamdrup and D. E. Canfield, *Limnol. Oceanogr.*, 1996, **41**, 1629–1650.
76 R. Dermott and M. Legner, *J. Great Lakes Res.*, 2002, **28**, 688–697.
77 R. Lauterborn, *Ber. Dtsch. Bot. Ges.*, 1907, **25**, 238–242.
78 M. Nishino, M. Fukui and T. Nakajima, *Water Res.*, 1998, **32**, 953–957.
79 N. M. Dul'tseva, S. M. Chernitsina and T. I. Zemskaya, *Microbiology*, 2012, **81**, 67–78.
80 B. B. Namsaraev, L. E. Dulov, G. A. Dubinina, T. I. Zemskaya, L. Z. Granina and E. V. Karabanov, *Microbiology*, 1994, **163**, 193–197.
81 M. G. Prokopenko, M. B. Hirst, L. De Brabandere, D. J. P. Lawrence, W. M. Berelson, J. Granger, B. X. Chang, S. Dawson, E. J. Crane Iii, L. Chong, B. Thamdrup, A. Townsend-Small and D. M. Sigman, *Nature*, 2013, **500**, 194–198.
82 A. W. Mackay, D. B. Ryves, R. W. Battarbee, R. J. Flower, D. Jewson, P. Rioual and M. Sturm, *Global Planet. Change*, 2005, **46**, 281–297.